



HAL
open science

Revisiting the strength of micron-scale ceramic platelets

Aurélien Doitrand, Ronan Henry, Jérôme Chevalier, Sylvain Meille

► **To cite this version:**

Aurélien Doitrand, Ronan Henry, Jérôme Chevalier, Sylvain Meille. Revisiting the strength of micron-scale ceramic platelets. *Journal of the American Ceramic Society*, 2020, 10.1111/jace.17148 . hal-02780475

HAL Id: hal-02780475

<https://hal.science/hal-02780475>

Submitted on 17 Jan 2021

HAL is a multi-disciplinary open access archive for the deposit and dissemination of scientific research documents, whether they are published or not. The documents may come from teaching and research institutions in France or abroad, or from public or private research centers.

L'archive ouverte pluridisciplinaire **HAL**, est destinée au dépôt et à la diffusion de documents scientifiques de niveau recherche, publiés ou non, émanant des établissements d'enseignement et de recherche français ou étrangers, des laboratoires publics ou privés.



Distributed under a Creative Commons Attribution 4.0 International License

Revisiting the strength of micron-scale ceramic platelets

Aurélien Doitrand^{a,*}, Ronan Henry^a, Jérôme Chevalier^a, Sylvain Meille^a

^a*Université Lyon, INSA-Lyon, MATEIS UMR CNRS 5510, F-69621 Villeurbanne Cedex, France*

Abstract

Individual platelets in nacre-like ceramics are able to locally withstand stress levels many times larger than the strength of larger specimens made of the same materials. This size effect, usually reported as being relative to the size of pre-existing defects, is described by considering both stress and energy failure conditions. We show that there is a characteristic length, defined by the material Young's modulus, fracture energy and strength, above which failure is governed by a stress criterion and below which energy considerations are dominant. Applying the coupled criterion to three-point bending of a single alumina platelet allows the identification of the platelet strength and fracture energy. The proposed approach also allows capturing the decrease in failure stress due to a surface defect accounting for its shape and size.

Keywords: Strength, fracture mechanics/toughness, failure, Nacre-like ceramics

1. Introduction

The interest towards nacre and nacre-like ceramics has been increasingly growing over the past years [1, 2, 3]. These bioinspired materials, generally manufactured from brittle constituents, combine high stiffness, strength and fracture toughness [2]. They consist of a dense packing of ordered and oriented micron-scale platelets [2, 4, 5, 6, 7, 8]. The orientation of the platelets along a specific direction can be achieved during the material manufacturing process by ice templating [2] or by adding ferro-magnetic particles that are sensitive to magnetic fields [5, 9]. Other manufacturing approaches can also be employed, such as ceramic layer gluing [10], or 3D printing [11]. The platelets are sintered and a secondary phase acts

like an interface that can consist of polymer [4, 5, 8], metal, ceramic [7], or also a glassy phase [2]. Bouville *et al.* [2] showed that varying the constituents of the secondary phase could lead to either brittle or non-brittle macroscopic mechanical behavior. The apparent non-brittle macroscopic mechanical behavior is mainly due to fracture mechanisms related to the material microstructure. Rather than propagating directly through the platelets, a crack is more likely to propagate in the secondary phase at the interface between the platelets, which causes crack deflection and branching [2, 11, 12]. Energy dissipation occurs through these mechanisms since larger crack surfaces are created than in the case of a straight crack that would penetrate through the platelets. An additional energy dissipation may also occur by means of local friction, thus resulting in a non-brittle macroscopic behavior.

The mechanical properties of the platelet and of the interface play a major role in the mechanical response of the material. Controlling the material microstructure is of primary importance in order to obtain mechanical properties that allow an optimal energy dissipation at the macroscopic scale, which could be achieved for instance by varying the platelet size or geometry. To this end, modeling interface and platelet failure may help to obtain guidelines to optimize the manufacturing process [13]. In particular, numerical simulation can be used to set up inverse approaches for the determination of interface strength and fracture toughness [14, 15]. Such approaches require the knowledge of the platelet mechanical behavior and properties used in fracture models such as, for instance, cohesive zone models [16, 17] phase field approach to fracture [18, 19, 20] or approaches based on Finite Fracture Mechanics (FFM) [21, 22].

The experimental determination of the platelet mechanical properties requires to (i) be able to perform micromechanical tests and (ii) set up post-processing approaches of these tests that provide the properties required as input in the models. Focused ion beam (FIB) allows manufacturing micron-scale specimens which can be mechanically tested thanks to micro-mechanical devices such as nano-indenters [23]. For instance, Pejchal *et al.* [24] performed flexural tests on microscopic alumina particle C-shaped and cantilever beam specimens. Based on the fracture location observed experimentally, they determined the maximum stress at this location from the finite element (FE) analyses, which was thus considered as the material strength. Maximum stress values as large as 10 GPa were obtained, decreasing

to 2 GPa in presence of defects. Similar tests were performed by Mueller *et al.* [28] in order to determine the strength of silicon particles in an aluminum alloy. Maximum stress levels between 7 and 15 GPa were obtained without apparent defects, and between 2 to 6 GPa in presence of defects. Following the same reasoning, Feilden *et al.* [3] determined that a single alumina platelet could locally sustain 5 GPa maximum stress under three-point bending.

In the three approaches mentioned above, the strength is defined as the maximum stress that the material can locally sustain before failure. It is obtained based on analytical or FE models that does not account for the possible flaws. In presence of a sharp flaw (crack, V-notch), the stress theoretically tends towards infinity, or at least reaches large values in the vicinity of the flaw. It is thus clear that this given definition of the strength does not allow characterizing a property that is specific to the material, since it depends on features such as, for instance, the specimen geometry or the presence of defects. Size effects in quasibrittle materials have been extensively investigated over the past decades to try to make a link between the strength of large and small structures [25, 26, 27]. .

The objective of this work is to provide insight regarding the high values of failure stress measured for single platelet by employing a framework in which the strength is considered as a characteristic of the material and does not depend on the geometry of the studied specimen. Section 2 is dedicated to the description of a failure prediction approach that combines stress and energy conditions. In Section 3, this approach is applied to obtain the failure stress of a single alumina platelet containing no flaws under tensile loading. Failure of a single platelet under three-point bending is modeled by FE in Section 4 in order to identify the platelet strength and toughness by confrontation to experimental measurements [3]. The influence of a flaw on the failure stress is also studied.

2. A criterion for crack initiation prediction

2.1. Stress and energy failure conditions

Following the approach proposed by Leguillon [21], we consider that the nucleation of a crack requires the simultaneous fulfillment of two conditions. The first condition describes the need for a sufficiently large local stress state to trigger crack initiation. It states that the stress normal to the crack path σ_{nn} must overcome the material strength σ_c over the entire

crack path before its nucleation. The second condition describes the need for a sufficiently large stored potential energy prior to crack initiation. It is derived from an energy balance between the energy dissipated by the crack nucleation ($-\Delta W = W(0) - W(S)$, where $W(S)$ is the potential energy corresponding to a crack of surface S) and the energy for new crack surface creation ($G_c S$, where S is the surface of the crack and G_c the material fracture energy). Both conditions can be expressed as non-dimensional expressions involving the crack surface S :

$$\begin{cases} \frac{\sigma_{nn}}{\sigma_c} \geq 1 \text{ along the presupposed crack path,} \\ \frac{G_{inc}(S)}{G_c} = \frac{-\Delta W(S)}{G_c S} \geq 1. \end{cases} \quad (1)$$

G_{inc} is the incremental energy release rate, which is usually an increasing function of the crack surface. Therefore, the second condition in Eqn. (1) provides a lower bound for the admissible crack surfaces at initiation. On the other side, the stress is generally a decreasing function of the distance to a stress concentrator in its vicinity, therefore the first condition in Eqn. (1) defines an upper bound for the admissible initiation crack surfaces. For a too small imposed loading, the stress criterion can be fulfilled for crack surfaces for which the incremental energy release rates are smaller than G_c . Moreover, the energy criterion can be fulfilled for crack surfaces for which the stress is smaller than σ_c . Therefore, the admissible crack initiation ranges provided by both criteria do not match and no crack surfaces satisfy both criteria simultaneously, as illustrated in Fig. 1a). Increasing the loading allows (i) increasing the crack surface upper bound provided by the stress criterion and (ii) decreasing the crack surface lower bound provided by the energy criterion, both bounds matching for a sufficiently large imposed loading which corresponds to the initiation loading (Fig. 1b)). The initiation loading is thus obtained as the minimum loading for which both criteria are simultaneously fulfilled for a given crack surface.

2.2. Application of the coupled criterion

The application of the coupled criterion (CC) for failure prediction requires several features. The stress state must be calculated for the configuration prior to crack initiation. This can be performed either based on analytical solutions [29, 30, 31] or employing Finite Element (FE) calculations (*cf.* Section 4). Thus, the stress condition can be computed, which allows determining the minimum loading required to fulfill the stress condition $P_s(S)$

as a function of the crack surface. The energy condition can be obtained by calculating the potential energy variation as a function of the crack surface, which allows determining the minimum loading required to fulfill this condition $P_e(S)$. The loading required to initiate a crack of a given surface S is determined as $P(S) = \max(P_s(S), P_e(S))$. The initiation surface S^* minimizes the loading required to fulfill both conditions:

$$S^* = \underset{S}{\operatorname{argmin}}(P(S)) = \underset{S}{\operatorname{argmin}}(\max(P_s(S), P_e(S))) \quad (2)$$

The initiation loading P^* can finally be determined as $P^* = P(S^*) = \max(P_s(S^*), P_e(S^*))$.

The input parameters required to apply the CC are the material constitutive behavior (Young's modulus and Poisson's ration for a linear elastic isotropic behavior) and its fracture energy G_c and strength σ_c . Therefore, it raises the question of a strength definition that is specific to the material, and does not depends on features such as the specimen geometry or the presence of external defects.

2.3. The strength to be used in the coupled criterion

The CC requires the material strength as an input to predict failure, which rises the question of defining the ceramic platelet strength, since it is well know that ceramic failure

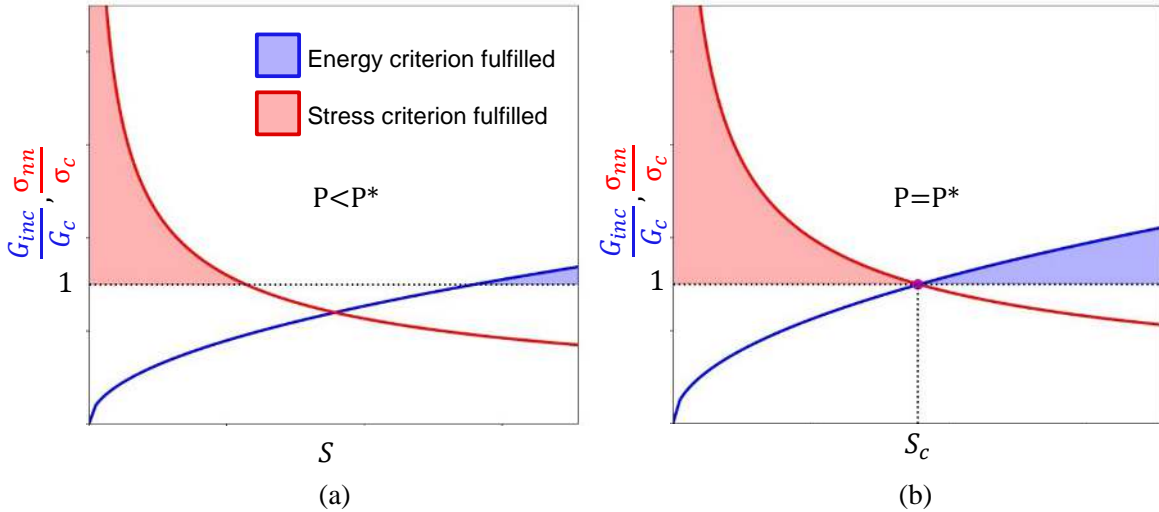


Figure 1: Stress to strength $\frac{\sigma}{\sigma_c}$ (solid red line) and incremental energy release rate to fracture energy $\frac{G_{inc}}{G_c}$ (solid blue line) ratios as a function of the crack surface S for an imposed loading P (a) lower than or (b) equal to the initiation load P^* . The filled area represents configurations for which the corresponding criterion is fulfilled.

stress strongly depends on the presence of flaws. Based on experimental work by Usami *et al.* [34] and Chantikul *et al.* [35], Leguillon *et al.* [32] recently proposed a definition for the strength to be used in the CC in the case of polycrystalline ceramics and studied the influence of a surface defect on the failure stress under tensile loading [33]. By studying the influence of an extrinsic (surface) flaw on the ceramic failure, they showed that (illustration of the results are given in Fig. 2):

- For a given grain size, the failure stress is governed by the flaw size for flaws larger than the grain size (Fig. 2a). However, a constant failure stress is obtained for extrinsic flaws smaller than the grain size, which allows defining an "intrinsic strength", *i.e.* a material property that does not depend on the extrinsic flaw size. The intrinsic strength is however governed by the grain size and the intrinsic flaws such as, *e.g.*, porosities (which size is, in first approximation, in the same order of magnitude as the grain size).
- For large grains in the absence of extrinsic flaws, the intrinsic strength follows a Hall-Petch-like law, *i.e.* the intrinsic strength varies as $\frac{1}{\sqrt{\Phi_G}}$, where Φ_G is the grain size (Fig. 2b).
- The intrinsic strength does not follow Hall-Petch for small grains (which would lead to high strength values) but reaches a plateau towards a value (called the "intrinsic strength")

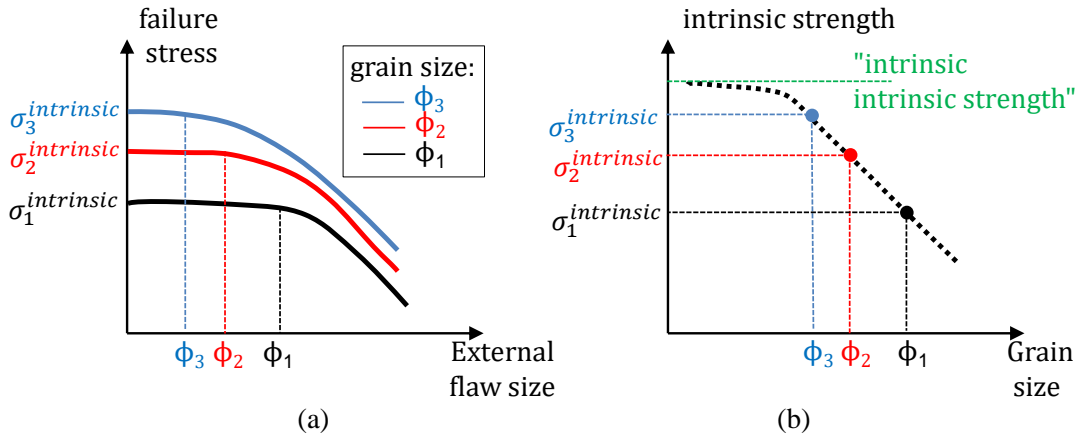


Figure 2: Log-log diagram of (a) failure stress of polycrystalline ceramics as a function of external flaw size for several grain sizes and (b) intrinsic strength as a function of the grain size.

intrinsic strength” [32]), which corresponds to the failure stress for a ceramic containing very small grains and flaws.

The ceramic platelet in nacre-like ceramics is a micron scale object containing relatively small (nanometric) intrinsic flaws. Hence, based on the abovementioned considerations, it appears that the strength value of a ceramic platelet that must be employed for the CC should be at least equal to the ”intrinsic strength”, *i.e.* the failure stress corresponding to the smallest possible grain size and intrinsic flaws. In the following, the influence of the strength on platelet failure prediction with the CC is studied and an estimate of both the platelet strength and fracture energy are identified by confrontation to experimental results available in the literature.

3. Failure of a single alumina platelet containing no flaws

Let us consider a single platelet subjected to uniaxial tensile loading (with a stress intensity σ_0). For the sake of simplicity, we consider a parallelepipedic platelet of length $2L$ and section $S = wt$ with a linear elastic behavior, *cf* Fig. 3. We first consider a platelet that does not contain any flaw (Fig. 3a). The stress state in the platelet is homogeneous and equal to the imposed stress σ_0 . Applying the stress conditions described in Section 2, we obtain a first necessary condition for the platelet failure:

$$\sigma_0 \geq \sigma_c \tag{3}$$

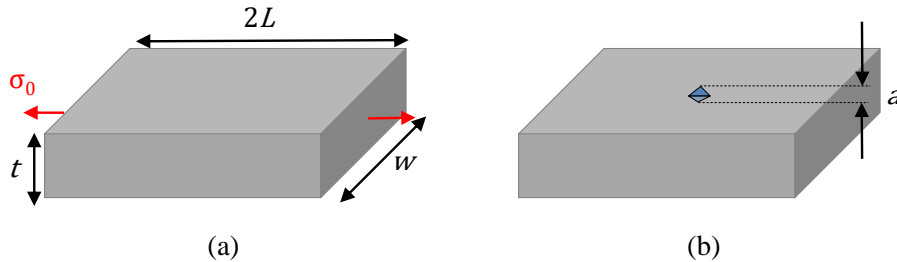


Figure 3: Schematic feature and dimensions of a platelet (a) without or (b) with a surface flaw.

where σ_c is the strength of the platelet constitutive material. Since the stress is homogeneous in the whole platelet, there is no preferential location for a crack to nucleate, such as in presence of a stress raiser (*e.g.* hole) or a singularity (*e.g.* crack, V-notch). Therefore, we assume that the platelet fails by suddenly breaking into two parts. It means that the potential energy after failure $W(S)$ is zero, thus the potential energy difference ΔW can be obtained from the potential energy of the platelet before failure $W(0)$:

$$-\Delta W = W(0) - W(S) = W(0) = \frac{1}{2} \int_V \underline{\underline{\sigma}} : \underline{\underline{\varepsilon}} dV = \frac{1}{2} \frac{\sigma_0^2}{E} 2LS, \quad (4)$$

where E is the platelet Young's modulus in the loading direction. Therefore, the energy condition given in Section 2 reads:

$$\frac{1}{2} \frac{\sigma_0^2}{E} 2LS \geq G_c S \quad (5)$$

which leads to a second condition for the platelet failure:

$$\sigma_0 \geq \sqrt{\frac{EG_c}{L}} \quad (6)$$

Fig. 4 shows the variation of the imposed stresses required to fulfill both criteria as a function of the platelet length. For a given platelet length, the failure stress σ_f is thus the maximum between both values, which corresponds to the minimum loading for which both criteria are simultaneously fulfilled. For long enough platelets, it can be seen that the platelet failure stress is equal to its constitutive material strength because there is more available energy than that necessary to fulfill the energy criterion. Therefore, the platelet breaks into two parts and the energy not consumed for the platelet failure is dissipated, for instance as kinetic energy (projection of the broken parts) or for supplementary crack surface creation (the platelet breaking into several parts). On the contrary, for small enough platelets, the platelet failure stress depends both on the platelet length and its constitutive material fracture energy. In this case, when the stress inside the platelet reaches the material strength, there is not enough stored energy to break the platelet so that it is necessary to increase the loading in order to fulfill the energy requirement. A sufficiently high imposed stress allowing the energy

criterion to be satisfied triggers the platelet failure, all the available energy being dissipated into crack surface creation. Combining both stress and energy requirements leads to defining a characteristic material length $L_{mat} = \frac{EG_c}{\sigma_c^2}$ for which the transition between both regimes occurs. For $2L < L_{mat}$, the energy criterion governs the platelet failure and the failure stress varies as $\frac{1}{\sqrt{L}}$ whereas for $2L > L_{mat}$ the platelet failure is governed by the material strength σ_c .

As a matter of example, let us consider 5 μm long Al_2O_3 platelets (corresponding to the average measured length for Ronafair[®] White Sapphire (Merck)). The platelet width and thickness are considered respectively as 5 μm and 1 μm . Typical mechanical properties of the constitutive material are $E = 300 \text{ GPa}$, $\nu = 0.21$, $G_c = 27 \text{ J/m}^2$ and $\sigma_c = 750 \text{ MPa}$ [32]. The strength is first chosen equal to the "intrinsic intrinsic strength" described in previous Section for illustrative purpose, an inverse identification approach for its determination is then proposed in Section 4. The corresponding material characteristic length is $L_{mat} = 14 \mu\text{m}$. Therefore, the failure stress of platelets larger than 14 μm would be equal to the strength σ_c . Since we consider platelets smaller than this characteristic length, failure is governed by the energy condition and thus depends on the platelet Young's modulus and

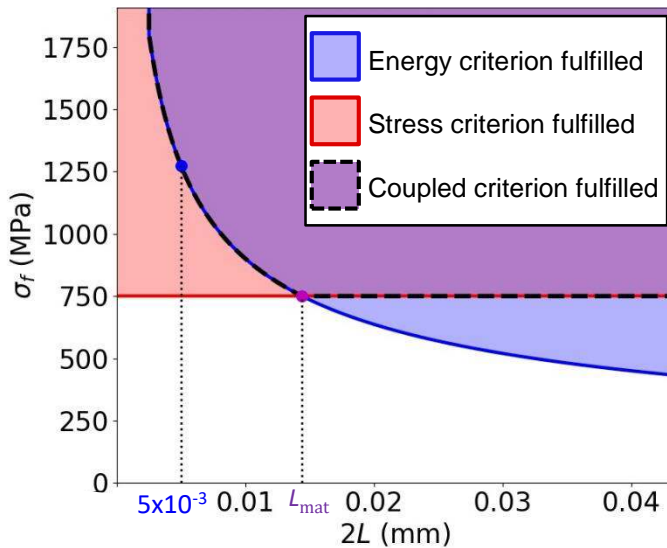


Figure 4: Failure stress σ_f as a function of the platelet length $2L$ predicted using (i) a stress criterion (solid red line), (ii) an energy criterion (solid blue line) and the coupled criterion (dashed black line). The filled area corresponds to couples $(2L, \sigma)$ for which the corresponding criterion is fulfilled.

fracture energy. The corresponding failure stress is given by Eqn. (6): $\sigma_f = 1.27$ GPa. It can be noted that this value is almost twice the material strength. This is not only due to the fact that the smaller the platelet, the lower the number and the size of flaws within it, which is a classical explanation to the outstanding platelet (apparent) strength measured experimentally. Indeed, we show here that the sole consideration of the platelet size allows explaining the increase in the failure stress, considering the same material properties for the platelet independently of its size. It can be noted that the platelet can locally withstand stress levels larger than its material constitutive strength. Indeed, in this case, failure cannot occur for stress levels corresponding to the characteristic strength because not enough energy is stored in the material.

4. Finite element model of platelet three-point bending

This section is dedicated to the platelet failure prediction under three-point bending using the criterion presented in Section 2.

4.1. FE model without flaws

A 2D plane strain FE model of three-point bending of a rectangular platelet is set up using AbaqusTM. Due to the specimen and test symmetry, we model only one half of the platelet. Boundary conditions are depicted in Fig. 5a. A point load is imposed on the platelet top node lying in the symmetry plane. The mesh consisting of 4-node linear elements

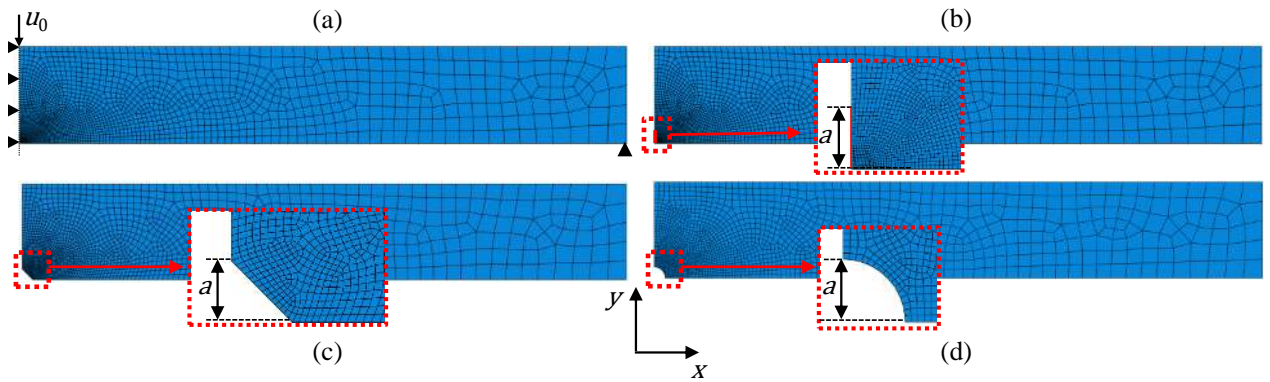


Figure 5: Typical FE mesh of half platelet containing (a) no flaws or a (b) crack, (c) V-notch or (d) semi circular surface flaw.

is refined in the vicinity of the specimen center, near the crack path corresponding to the location where the stress variation is computed in order to determine the stress criterion. This mesh refinement is required in order to catch the crack initiation length, which is not known a priori. Nevertheless, it can be shown that this length is a fraction of the material characteristic length $L_{mat} = \frac{EG_c}{\sigma_c^2}$ [33]. We consider herein a simplified linear elastic isotropic behavior for the platelets, with $E = 300$ GPa and $\nu = 0.21$. First, typical fracture energy values for isotropic alumina is used: $G_c = 27$ J/m² [32]. Then, an approach is proposed to identify this value as well as the platelet strength. The influence of the strength on the platelet failure is studied in the following. The minimum element size is defined as $\frac{L_{mat}}{30}$ in order to ensure that the crack initiation length is captured by the proposed simulations. Typical meshes used for the simulations contain around 5000 degrees of freedom. The coupled criterion application is first based on the calculation of the energy criterion, which requires the calculation of the potential energy variation to be computed for several crack lengths. The meshes containing cracks with different lengths are obtained by successively removing the symmetry condition for the nodes lying on the crack path. Then, the stress condition can be calculated by computing the tensile stress variation along the presupposed crack path based on a mesh without crack. Once the tensile stress σ_{nm} and potential energy W variations are obtained, only a post-processing is required to determine the minimum loading for which both the stress and the energy conditions are satisfied, *i.e.* the initiation load.

4.2. Numerical prediction of failure stress

The FE model presented in Section 4.1 is now used in order to predict single alumina platelet failure under three-point bending. Experimental measurements taken from [3] are considered herein. The dimensions of ten tested platelets are given in Tab. 1 as well as the measured failure forces. Local stress levels as large as 5 GPa may be reached at the platelet surface, which is consistent with the results obtained in [3]. Of course, since the upper half of the platelet undergoes compression, the stress is null in the platelet center in the thickness direction.

Fig. 6 displays the variation of the stress to strength and incremental energy release rate to fracture energy ratios as a function of the crack length corresponding to specimen #10

Specimen	1	2	3	4	5	6	7	8	9	10
$2L$ (μm)	5.30	5.65	5.65	5.57	5.57	5.57	5.57	5.57	5.57	5.57
t (μm)	0.41	0.60	0.87	0.94	0.43	0.51	0.44	0.51	0.50	0.79
w (μm)	2.58	2.12	2.76	3.18	2.78	2.15	5.02	3.82	3.30	3.35
F_c^e (μN) - experiments	0.34	0.65	1.14	1.07	0.39	0.24	0.67	0.63	0.38	1.61
F_c^n (μN) - predictions	0.29	0.45	1.10	1.46	0.34	0.35	0.69	0.62	0.52	1.15

Table 1: Platelet dimensions and failure force (i) measured experimentally under three-point bending [3] and (ii) predicted numerically with the coupled criterion.

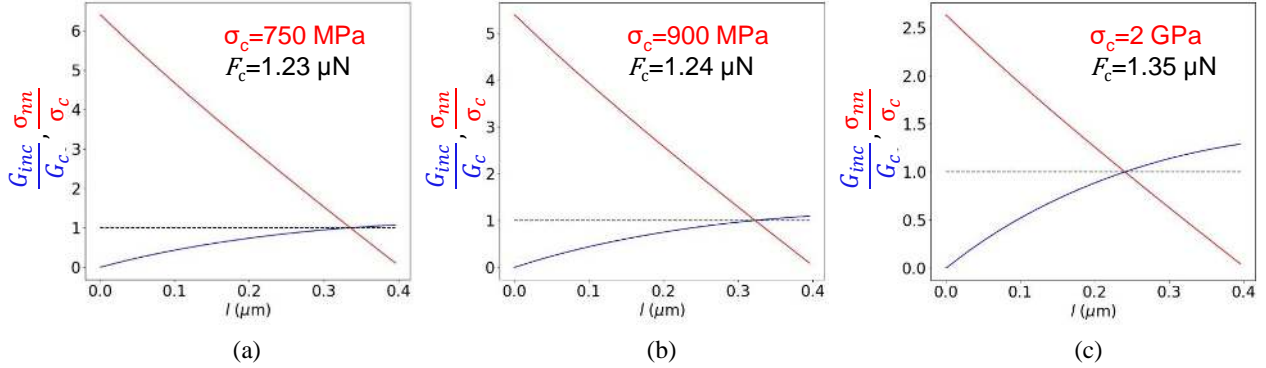


Figure 6: Incremental energy release rate to fracture energy (blue curve) and normal stress to strength ratios (red curve) as a function of the crack length for specimen #10 for $G_c = 27 \text{ J/m}^2$ a) $\sigma_c = 750 \text{ MPa}$, b) $\sigma_c = 900 \text{ MPa}$ and c) $\sigma_c = 2 \text{ GPa}$.

with a 0.79mm thickness for different intrinsic strength. Depending on the strength value, two failure regimes can be distinguished (Fig. 6):

- For small enough strength values ($\sigma_c \leq 900 \text{ MPa}$, Fig. 6a-b), it can be seen that the stress state in the platelet overcomes the material strength over almost all the area undergoing tension (*i.e.* for $l < \frac{t}{2} \approx 0.4 \mu\text{m}$). Therefore, failure is driven by the energy condition since the stress criterion could be fulfilled for smaller imposed loadings, however the energy criterion would not be fulfilled and hence failure would not occur. Such a configuration has already been encountered in other situations, such as, for instance, in the case of transverse cracking in composite materials [36, 37]. In this case, the failure load F_c corresponds to the loading required to fulfill the energy criterion, which is larger than that required to fulfill the stress criterion. The failure load thus mainly depends on the fracture energy and almost does not depend on the strength. In this case, micromechanical tests such as three-point bending of micron-scale platelet

allows determining the material fracture energy rather than its strength.

- For larger strength values (*e.g.* $\sigma_c = 2$ GPa, Fig. [6c](#)), the failure load predicted by the CC both depends on the material fracture energy and strength. This is consistent with results obtained in Section [3](#) since larger strength value leads to smaller values of L_{mat} and hence smaller ranges of platelet length for which the failure is only driven by the energy condition.

In both cases, stress levels larger than σ_c are locally attained. Nevertheless, it is shown herein that this local stress level does not define the platelet strength. Such stress levels are reached because the imposed loading must be sufficiently high so that there is enough stored elastic energy available to be dissipated for the platelet failure. Therefore, the platelet failure is not only driven by its strength but also by its fracture energy.

4.3. Fracture energy and strength identification

The CC allows the prediction of the failure force providing the knowledge of the material strength and fracture energy. If these parameters are not known, it can also be used as a way to determine it by indirect confrontation to experimental measurements. The identification approach consists in determining the parameter couple (G_c, σ_c) that minimizes the residuals R quantifying the difference between predicted and measured failure forces obtained for N specimens:

$$R^2(G_c, \sigma_c) = \sum_{i=1}^N (F_i^n(G_c, \sigma_c) - F_i^e)^2, \quad (7)$$

where $F_i^n(G_c, \sigma_c)$ is the failure force predicted numerically with the coupled criterion for the specimen #i employing the strength σ_c and fracture energy G_c , and F_i^e is the force at failure measured experimentally for the same specimen. The minimization problem that must be solved writes:

$$\text{Find } (G_c^*, \sigma_c^*), R(G_c^*, \sigma_c^*) = \min_{G_c, \sigma_c} R(G_c, \sigma_c). \quad (8)$$

Solving this minimization problem requires the calculation of the failure force corresponding to each specimens for several couples (G_c, σ_c) either to set up a gradient descend approach or to compute the residuals variation for a priori chosen couples of parameters. The failure force calculation is obtained employing the coupled criterion, which requires some FE calculations

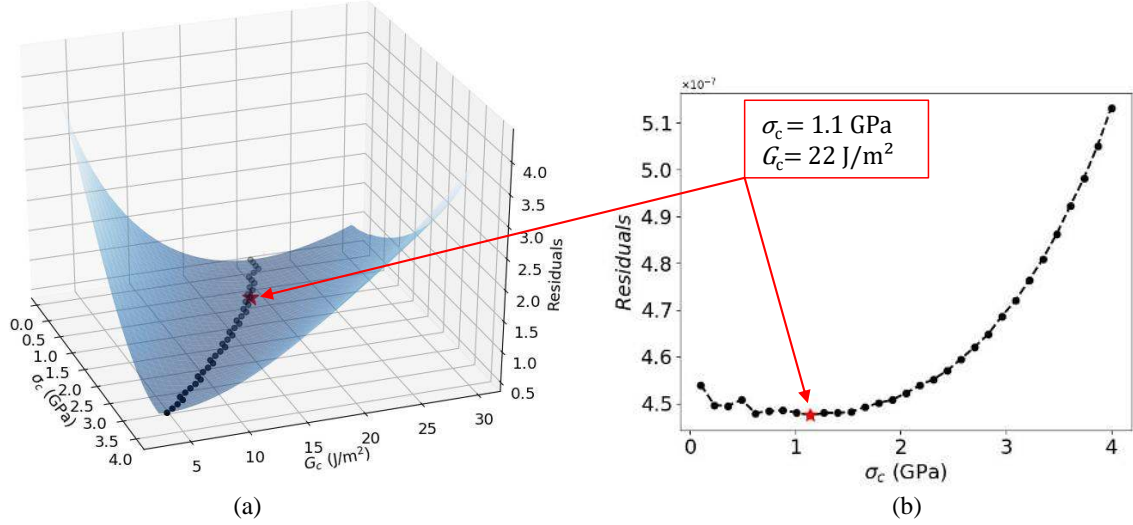


Figure 7: Residuals as a function of (a) fracture energy and strength and (b) strength corresponding to the residuals minimum obtained for a fixed strength value (black dots in b) corresponds to those depicted in a)).

to compute the incremental energy release rate and the stress variation (*cf.* Section 4.1). It can be noted that a major advantage of the CC is the possibility to vary (G_c, σ_c) without any extra FE calculations since these parameters are only implemented during the post-processing step. The minimization procedure thus only requires post-processing FE calculations, which is computationally very efficient compared to other approaches such as, *e.g.*, cohesive zone modeling [16, 17] or phase field [18, 19, 20], which would require as many FE calculations as the number of chosen (G_c, σ_c) couples. Fig. 7a displays the residuals variation as a function of G_c and σ_c . The black dots indicate the residuals minimum for a fixed strength (corresponding to the fracture energy that minimize the difference between predicted and measured failure stress for this strength), which are also reported in Fig. 7b. It can be observed first that for small enough strength value (below around 2 GPa), the residuals minimum is reached for the same value of G_c . As already explained previously (*cf.*, *e.g.* Fig. 6a-b), it corresponds to a regime for which failure is mainly driven by the fracture energy, therefore similar fracture energy (G_c between 20 and 25 J/m²) is obtained regardless the strength. For larger strengths, it appears that failure is driven both by fracture energy and strength, thus the fracture energy corresponding to the residuals minimum obtained for a given strength decreases with increasing strength (Fig. 7a). As observed in Fig. 7b, the residuals increase with increasing strength above 2 GPa, which indicates that such strength values lead to a worse agreement

between predicted and measured failure forces. The parameter couple that leads to the best agreement with experimental data is ($G_c=22 \text{ J/m}^2, \sigma_c=1.1 \text{ GPa}$). It can be noted that a similar agreement is obtained for strength values between 500MPa and 1.5GPa, which is traduced by relatively flat residuals for this strength range. The corresponding fracture energy range is 20-25 J/m^2 .

It can be seen that the identified strength value is a slightly larger than the alumina "intrinsic intrinsic strength". This is not surprising since the latter corresponds to a configuration with very small grains and flaws, however still possibly including intrinsic microstructural features such as grain boundaries, small porosities that could be privileged locations for crack initiation. The forces at failure predicted numerically employing the coupled criterion F_c^n for the ten specimens are summarized in Table [1](#) for ($G_c=22 \text{ J/m}^2, \sigma_c=1.1 \text{ GPa}$). It can be seen that a good estimate of the failure force is obtained employing the proposed approach. The deviation between numerically predicted and experimentally measured failure force is within 20% for all the considered specimens.

4.4. Possible surface flaws

The common explanation for the large measured platelet failure stress is based on the fact that the smaller the platelet the smaller the flaws, that may be privileged locations for crack initiation. We demonstrated in the previous sections that due to its small dimensions, according to the CC, the platelet failure stress is actually driven by both its strength and fracture energy and reaches large values because of its size that is smaller than the material characteristic length. This section is dedicated to the influence of a surface flaw on platelet failure. We consider three possible kinds of flaws: a crack, a V-notch or a semi-circular flaw. The same method as described in Section [4.1](#) can be employed in order to predict failure in presence of a flaw. The stress along the presupposed crack path and the potential energy for several crack lengths are computed, which allows applying the coupled criterion so as to determine the failure load. Fig. [8](#) displays the force at failure ratio in presence of and without a surface flaw as a function of flaw size to platelet thickness ratio for V-notch, semi-circular or crack-like flaw. It can be first seen that the larger the surface flaws, the smaller the failure force independently of the flaw shape. Moreover, for small enough flaw sizes, the influence of the flaw shape on the force at failure is not marked. For large enough flaws, the influence of

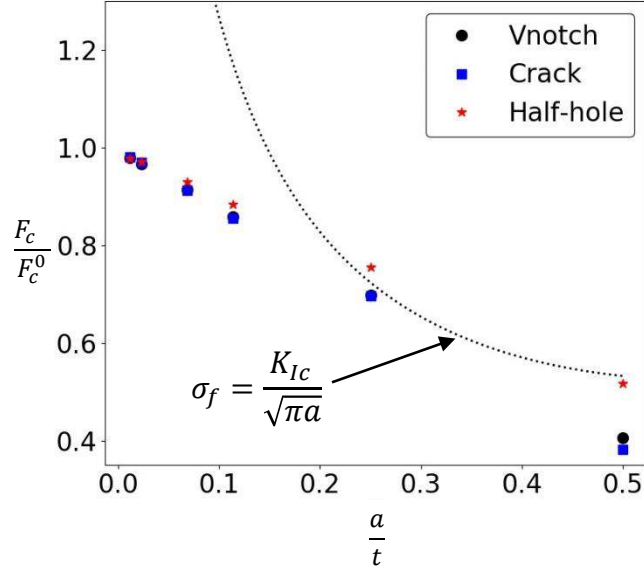


Figure 8: Ratio between force at failure in presence of (F_c) and without (F_c^0) a surface flaw of different kind (V-notch, half-hole or crack). The grey dashed line corresponds to the failure force predicted based on linear elastic fracture mechanics.

the flaw shape is highlighted since the failure force is smaller in the case of a crack than for a V-notch or for a semi-circular hole. It is consistent with the conclusions drawn by Martin *et al.* [33] who highlighted the small influence of flaw shape for flaws smaller than $\frac{L_{mat}}{2}$ under tensile loading. We also display on Fig. 8 the force at failure obtained using the classical explanation based on linear elastic fracture mechanics that the smaller the defects, the higher the failure stress (gray dashed line). This failure stress is computed as $\sigma_f = \frac{K_{Ic}}{\sqrt{\pi a}}$. Then, the failure force is estimated as the force for which the maximum stress reached locally in the platelet is σ_f , following the approach described for instance in [3, 24, 28]. This approach provides failure forces in the same order of magnitude as those obtained with the CC for large enough flaw size. However, the predicted failure force deviates from that obtained with the CC for small flaws since it tends towards infinity for infinitesimal flaws.

The order of magnitude of the flaw size estimated based on experimental data in alumina platelets is around 30 nm [3]. For the platelets under investigation, it leads to a flaw size to platelet thickness ratio between 0.032 and 0.073, which corresponds to a maximum failure force decrease predicted by the CC smaller than 10% compared to the failure force obtained for a platelet containing no flaw.

5. Conclusion

The high failure stress of a single alumina platelet results from its dimensions compared to its constitutive material characteristic length. Considering both energy and stress failure conditions allows predicting the platelet failure loading under three-point bending. The proposed approach requires the knowledge of the platelet Young's modulus, fracture energy and strength, these parameters being considered as intrinsic to the constitutive material and independent from the studied structure size or the possible presence of external flaws. The platelet failure is driven either by only the material fracture energy, or by both its strength and fracture energy. In the case of specimens smaller than the material characteristic length, the energy condition requires substantially high loading to be met compared to the loading required to fulfill the stress condition. The platelet can thus undergo local stress levels several times larger than its constitutive material strength.

The coupled criterion allows the inverse identification of a single alumina platelet strength and fracture energy by confrontation of predicted and measured failure stress under three-point bending. The proposed approach also allows evaluating the influence of a surface defect on the failure force. It is worth pointing out that the proposed approach is not inconsistent with statistical approaches to failure, such as Weibull theory. Both approaches can even be combined so as to predict failure [38].

It finally appears that micromechanical tests, such as three-point bending of a single ceramic platelet, can be employed in order to determine the platelet fracture energy and possibly its strength. The platelet smallness allows it to withstand high local stress levels compared to the strength of their constitutive material because failure requires a sufficient amount of energy to be stored so that it can be released into crack surface creation energy.

6. References

References

- [1] Berthelat F, Tang H, Zavattieri PD, Li CM, Espinosa HD. On the mechanics of mother-of-pearl: A key feature in the material hierarchical structure. *J Mech Phy Sol*

2007;55:306-337 .

- [2] Bouville F, Maire E, Meille S, Van de Moortèle B., Stevenson A.J., Deville S. Strong, tough and stiff bioinspired ceramics from brittle constituents. *Nat Mater* 2014;13:508–514.
- [3] Feilden E, Giovannini T, Ni N, Ferraro C, Saiz E, Vandeperre L *et al.*. Micromechanical strength of Al₂O₃ platelets. *Scripta Mater* 2017;131:55-58.
- [4] Bonderer LJ, Studard A, Gauckler LJ. Bioinspired design and assembly of platelet reinforced polymer films. *Science* 2008;319:1069–1073.
- [5] Erb RM, Libanori R, Rothfuchs N, Studart AR. Composites reinforced in three dimensions by using low magnetic fields. *Science* 2012;335:199-204.
- [6] Kotoul M, Pokluda J, Šandera P, Dlouhý I, Chlup Z, Boccaccini AR. Toughening effects quantification in glass matrix composite reinforced by alumina platelets. *Acta Mater* 2008;56:2908–2918.
- [7] Le Ferrand H, Bouville F, Niebel TP, Studart AR. Magnetically assisted slip casting of bioinspired heterogeneous composites. *Nat Mater* 2015;14:1172-1181.
- [8] Shukla DK, Kasisomayaajula SV, Parameswaran V. Epoxy composites using functionalized alumina platelets as reinforcements. *Compos Sci Technol* 2008;68(14):3055–3063.
- [9] Meyers MA, McKittrick J, Chen PY. Structural biological materials: Critical mechanics-materials connections. *Science* 2013;339:773-779.
- [10] Clegg WJ, Kendall K, Alford NM, Button TW, Birchall JD. A simple way to make tough ceramics. *Nature* 1990;347:455-457.
- [11] Feilden E, Ferraro C, Zhang Q, García-Tunon E, D’Elia E, Giuliani F *et al.*. 3D Printing Bioinspired Ceramic Composites. *Sci Rep* 2017;7:13759.
- [12] Picot OT, Rocha VG, Ferraro C, Ni N, D’Elia E, Meille S *et al.*. Using graphene networks to build bioinspired self-monitoring ceramics. *Nature comm* 2017;8:14425.

- [13] Radi K, Jauffrès D, Deville S, Martin CL. Elasticity and fracture of brick and mortar materials using discrete element simulations. *J Mech Phy Sol* 2019;126:101–116.
- [14] Doitrand A, Leguillon D. 3D application of the coupled criterion to crack initiation prediction in epoxy/aluminum bimaterial specimens under four point bending. *Int J Sol Struct* 2018;143:175-182.
- [15] Doitrand A, Leguillon D Comparison between 2D and 3D applications of the coupled criterion to crack initiation prediction in scarf adhesive joints. *Int J Adh and Adh* 2018;85:69-76.
- [16] Barenblatt G. The formation of equilibrium cracks during brittle fracture. General ideas and hypotheses. Axially-symmetric cracks. *J App Math Mech* 1959;23:622–636.
- [17] Dugdale DS. Yielding of steel sheets containing slits, *J Mech Phy Sol* 1960;8:100–104.
- [18] Bourdin B, Francfort GA, Marigo JJ. Numerical experiments in revisited brittle fracture, *J Mech Phy Sol* 2000;48:797–826.
- [19] Miehe C, Welschinger F, Hofacker M. Thermodynamically consistent phase-field models of fracture: Variational principles and multi-field FE implementations, *Int J Numer Meth Engng* 2010;83:1273–1311.
- [20] Molnár G, Gravouil A. 2D and 3D Abaqus implementation of a robust staggered phase-field solution for modeling brittle fracture, *Fin Elem Anal Des* 2017;130:27–38.
- [21] Leguillon D. Strength or toughness? A criterion for crack onset at a notch. *Eur J Mech A/Sol* 2002;21:61-72.
- [22] Weissgraeber P, Leguillon D, Becker W. A review of Finite Fracture Mechanics: crack initiation at singular and non-singular stress-raisers. *Arch Appl Mech* 2016;86:375-401.
- [23] Di Maio D, Roberts SG. Measuring fracture toughness of coatings using focused-ion-beam-machined microbeams. *J Mat Res*, 2005;20(02):299–302.
- [24] Pejchal V, Fornabaio M, Žagar G, Mortensen, A., A. The local strength of individual alumina particles. *J Mech Phy Sol* 2017;109:34-49.

- [25] Bažant ZP. Instability, ductility, and size effect in strain-softening concrete. *ASCE J Eng Mech Div* 1976;102(2):331-344.
- [26] Bažant ZP. Size effect in blunt fracture: concrete, rock, metal. *J engng mech* 1984;110(4):518-535.
- [27] Bažant, Z.P.. Scaling theory for quasibrittle structural failure. *Proceedings of the National Academy of Sciences* 2004;101(37):13400-13407.
- [28] Mueller MG, Žagar G, Mortensen, A. In-situ strength of individual silicon particles within an aluminium casting alloy. *Acta Mater* 2018;143:67-76.
- [29] Westergaard HM. Stresses at a crack, size of the crack and the bending of reinforced concrete. *Proc American Concrete Institute* 1934;30:93-102.
- [30] Doitrand A, Martin E, Leguillon D. Numerical implementation of the coupled criterion: Matched asymptotic and full finite element approaches. *Fin Elem Anal Des* 2020;168:103344.
- [31] Cornetti P, Sapora A, Carpinteri A. Mode mixity and size effect in V-notched structures. *Int J Sol Struct* 2013;50(10):1562-1582.
- [32] Leguillon D, Martin E, Seveček O, Bermejo R. What is the tensile strength of a ceramic to be used in numerical models for predicting crack initiation? *Int J Fract* 2018;212(1):89-103.
- [33] Martin E, Leguillon D, Seveček O, Bermejo R. Understanding the tensile strength of ceramics in the presence of small critical flaws. *Engng Frac Mech* 2018;201:167-175.
- [34] Usami S, Kimoto H, Takahashi I, Shida S. Strength of ceramic materials containing small flaws. *Engng Fract Mech* 1986;23:745–761.
- [35] Chantikul P, Bennison SJ, Lawn BR. Role of grain size in the strength and R-curve properties of alumina. *J Am Ceram Soc* 1990;73:2419–2427.

- [36] Doitrand A, Fagiano C, Carrère N, Chiaruttini V, Hirsekorn M. Damage onset modeling in woven composites based on a coupled stress and energy criterion. *Engng Fract Mech* 2017;169:189–200.
- [37] García IG, Carter BJ, Ingraffea AR, Mantič V. A numerical study of transverse cracking in cross ply laminates by 3D finite fracture mechanics. *Compos Part B* 2016;95:475–87.
- [38] Leguillon D, Martin E, Lafarie-Frenot MC. Flexural vs. tensile strength in brittle materials. *Comptes Rendus Mecanique* 2015;43(4):275-281.